Available on the CERN CDS information server **CMS PAS QCD-10-015**

CMS Physics Analysis Summary

Contact: cms-pag-conveners-qcd@cern.ch 2010/07/23

Dijet Azimuthal Decorrelations and Angular Distributions in pp Collisions at $\sqrt{s} = 7$ TeV

The CMS Collaboration

Abstract

We present a study of dijet azimuthal decorrelations and angular distributions in pp collisions at $\sqrt{s}$ = 7 TeV using the CMS detector. The analyses are based on an inclusive dijet event sample that corresponds to 72 nb^{-1} of integrated luminosity. The results are compared to predictions from Monte Carlo event generators and perturbative QCD calculations. The sensitivity of the dijet azimuthal distributions to the phenomenological parameters used to model initial and final-state QCD radiation is also investigated.

1 Introduction

Within the framework of Quantum Chromodynamics (QCD), high-energy inelastic collisions at high momentum transfers between protons are described as a point-like scattering between the proton constituents, which are collectively referred to as partons. After the collision, the outgoing partons manifest themselves, via soft quark and gluon radiation and hadronization processes, as localized streams of particles, identified as jets. The production of events containing two jets with large transverse momenta (dijets) is one of the basic QCD processes occurring at hadron colliders. Measurements of angular distributions in azimuth and in polar scattering angle can provide tests of QCD and a probe of new physics. In this note we present the first preliminary measurements of dijet azimuthal decorrelations and dijet angular distributions in pp collisions at $\sqrt{s} = 7$ TeV.

The azimuthal angle, $\Delta\varphi_{\text{dijet}} = \left|\varphi_{\text{jet1}} - \varphi_{\text{jet2}}\right|$, between the two highest transverse momentum (leading) jets in hard-scattering events can be used to study higher-order QCD radiation effects without the need to explicitly reconstruct additional jets. The study of dijet azimuthal decorrelations provides an ideal testing ground for perturbative QCD (pQCD) calculations and Monte Carlo (MC) event generators over a wide range of jet multiplicities, and offers a way to study the transition between soft and hard QCD processes [1]. At leading order (LO), the two jets have equal transverse momenta with respect to the beam axis ($\mathrm{p_T}$) and are completely correlated in the azimuthal angle ($\Delta\varphi_{\text{dijet}} = \pi$). However, soft-gluon emissions in the initial and final states will decorrelate the two leading jets and will cause small deviations from π. Large deviations from π also occur in the case of hard multi-jet production. Three-jet topologies dominate the region of $2\pi/3 < \Delta\varphi_{\text{dijet}} < \pi$, whereas, angles smaller than $2\pi/3$ are populated by four-jet events. The observable is defined as the event-normalized differential dijet distribution in $\Delta\varphi_{\text{dijet}}$, $(1/\mathrm{N})(d\mathrm{N}/d\Delta\varphi_{\text{dijet}})$. By normalizing the $\Delta\varphi_{\text{dijet}}$ distributions in this manner, many experimental uncertainties are significantly reduced. Measurements of differential dijet azimuthal cross sections at central rapidities have previously been reported at the Tevatron by the DØ collaboration [2].

The dijet angular distribution probes the properties of parton-parton scattering without strong dependence on the details of the parton distribution functions; since all three classes of scattering processes are dominated by t-channel gluon exchange, the angular dependence of the $qg \to qg$, $q\bar{q}(q') \to q\bar{q}(q')$, and $gg \to gg$ processes are similar. The dijet angular distribution is typically expressed in terms of $\chi_{\text{dijet}} = \exp(|\mathrm{y}_1 - \mathrm{y}_2|)$, where y_1 and y_2 are the rapidities of the two leading jets, and $\mathrm{y} = \frac{1}{2}\ln\left[(\mathrm{E} + \mathrm{p}_z) \,/\, (\mathrm{E} - \mathrm{p}_z)\right]$, where E is the energy of the jet and p_z is the projection of the jet momentum on the beam axis. This choice of χ_{dijet} is motivated by the fact that it has a flat distribution for t-channel gluon exchange sub-processes. It also allows signatures of new physics that might have a more isotropic angular distribution than QCD (e.g., quark compositeness) to be more easily examined as they would produce an excess at low values of χ_{dijet}. The observable is defined as the event-normalized differential dijet distribution in χ_{dijet}, $(1/\mathrm{N})(d\mathrm{N}/d\chi_{\text{dijet}})$. Measurements of dijet angular distributions have previously been reported at the Tevatron by the DØ [3, 4] and CDF [5] collaborations.

The Compact Muon Solenoid (CMS) detector is described in detail elsewhere [6]. In this study, jets are identified using energy depositions from the lead-tungstate crystal electromagnetic calorimeter and the brass-scintillator hadronic calorimeter. These calorimeters provide a uniform and hermetic coverage over a large range of pseudorapidity ($|\eta| \leq 5$, where $\eta = -\ln\tan(\theta/2)$ and θ is the polar angle relative to the proton beam.) The calorimeter cells are grouped in projective towers of granularity $\Delta\eta \times \Delta\varphi = 0.087 \times 0.087$ at central, with coarser segmentation at forward rapidities. CMS uses a right-handed coordinate system, with the origin located at the

nominal collision point, the x-axis pointing towards the center of the LHC, the y-axis pointing up (perpendicular to the LHC plane), and the z-axis along the anticlockwise beam direction.

CMS uses a two-tiered trigger system to select events online; Level-1 (L1) and the High Level Trigger (HLT). Events were selected using two inclusive single-jet triggers that required a L1 jet with $p_T > 6$ GeV (20 GeV) and an HLT jet with $p_T > 15$ GeV (30 GeV). We refer to these triggers as HLT15 and HLT30. The jet energies used in the triggers were not corrected for calorimeter energy response. Events were required to have a primary vertex reconstructed along the beam line and within 15 cm from the detector center. Cleaning cuts were applied to reject beam halo events and to remove events whose timing was not consistent with the LHC bunch crossing. The data sample used correspond to an accumulated integrated luminosity of 72 nb^{-1}.

Jets were reconstructed offline from calorimeter energy depositions using the anti-k_T clustering algorithm [7] with a distance parameter $R = 0.5$. Spurious jets from isolated noisy calorimeter cells were eliminated by loose quality cuts on the jet properties [8]. The jet four-vectors were corrected for energy response of the calorimeter as determined from a PYTHIA [9] MC sample passed through a GEANT4 [10]-based simulation of the CMS detector [11]. The jet p_T resolutions were determined from MC truth information and verified with collision data [11].

2 Dijet Azimuthal Decorrelations

Events were required to have two leading jets with rapidity $|y| \leq 1.1$ and $p_T > 30$ GeV. The transverse momentum of the leading jet in the event (p_T^{max}) was required to be greater than 70 GeV, which is above the p_T threshold of 57 GeV at which the HLT30 trigger was fully efficient. After all selection cuts a sample of 40579 events remained.

The event-normalized differential dijet distributions in $\Delta\varphi_{dijet}$ are shown in Fig. 1 in four p_T^{max} regions. The distributions are scaled by multiplicative factors for purposes of presentation. The $\Delta\varphi_{dijet}$ distributions are strongly peaked at π and become narrower with increasing p_T. The $\Delta\varphi_{dijet}$ distributions from the PYTHIA (D6T tune), HERWIG++ [12], and MADGRAPH [13] event generators are also presented for comparison. The MADGRAPH generator is based on LO Matrix Element multi-parton final state predictions, using PYTHIA for parton showering and hadronization. The data have not been corrected for event migration effects due to the finite jet energy and position resolutions of the detector. These detector resolution effects have been included in the MC predictions.

Sources of systematic uncertainty arise from uncertainties in the jet energy calibration and the jet p_T resolution. The sensitivity of the measurement to the jet energy correction uncertainty was estimated by varying the overall energy correction of calorimeter jets by $\pm 10\%$ and by $\pm 2\%$ linearly per unit of $|\eta|$ [11]. Ratios between the $\Delta\varphi_{dijet}$ distributions, using a PYTHIA MC sample, from the nominally corrected calorimeter jets and from the calorimeter jets with varied jet energies were used to estimate the effect of this uncertainty for each $\Delta\varphi_{dijet}$ bin and p_T^{max} region. Similarly, the sensitivity of the jet energy resolution uncertainty on the dijet azimuthal distributions was examined by varying the jet p_T resolutions by $\pm 10\%$ [11] in the PYTHIA MC and comparing the $\Delta\varphi_{dijet}$ distributions before and after the change. The combined systematic uncertainty, constructed by taking the quadratic sum of the jet energy calibration and resolution uncertainties, varies from $\sim$25% at $\Delta\varphi_{dijet} = \pi/2$ to $\sim$ 5% at $\Delta\varphi_{dijet} = \pi$.

Figure 2 shows the ratios of the data dijet azimuthal distributions to the predictions of PYTHIA, HERWIG++, and MADGRAPH in p_T^{max} regions. The combined systematic uncertainty is shown by the shaded band. The predictions from PYTHIA and HERWIG++ are in reasonable agreement

with the data. MADGRAPH predicts about 20% less azimuthal decorrelation, for $\Delta\varphi_{\text{dijet}}$ away from π, than what is observed in the data.

The sensitivity of the $\Delta\varphi_{\text{dijet}}$ distributions to QCD initial-state radiation (ISR) and final-state radiation (FSR) effects is investigated by varying the multiplicative parameters that control the amount of ISR (k_{ISR} = *PARP(67)*) and FSR (k_{FSR} = *PARP(71)*) in PYTHIA. Figure 3 shows comparisons of the $\Delta\varphi_{\text{dijet}}$ distributions from data to PYTHIA distributions with increased (decreased) ISR which correspond to k_{ISR} of 1.0 (4.0). The default value of k_{ISR} in PYTHIA tune D6T is 2.5. The effects are more visible for lower jet $\mathrm{p_T^{max}}$ and for smaller $\Delta\varphi_{\text{dijet}}$ angles. The variation of k_{FSR} between 2.5 and 8.0 (default value is 4.0) causes very small effects in all leading jet $\mathrm{p_T^{max}}$ regions, as shown in Fig. 4. These results indicate that the differential dijet azimuthal distributions could be used to tune parameters in MC event generators that control radiative effects in the initial state.

3 Dijet Angular Distributions

Events having two leading jets with rapidities $\mathrm{y_1}$ and $\mathrm{y_2}$ were selected. We define the mean $\mathrm{y_{boost}} = \frac{1}{2}|\mathrm{y_1} + \mathrm{y_2}|$ and the half difference $\mathrm{y^*} = \frac{1}{2}|\mathrm{y_1} - \mathrm{y_2}|$. In the limit of massless $2 \to 2$ scattering processes, the scattering angle θ^* at the parton-parton (i.e., dijet) center-of-mass (CM) frame can be expressed as $\theta^* = \cos^{-1}(\tanh \mathrm{y^*})$, where $\pm\mathrm{y^*}$ are the rapidities of the two jets in the dijet CM frame, and $\mathrm{y_{boost}}$ is the longitudinal boost of the dijet CM frame with respect to the proton-proton CM frame. In this limit the $\chi_{\text{dijet}} = \exp(2\mathrm{y^*}) = (1 + \cos\theta^*)/(1 - \cos\theta^*)$.

The dijet angular distributions are measured as a function of χ_{dijet} in different regions of the dijet invariant mass, M_{jj}. Both the HLT15 and HLT30 trigger were used in the analysis. The HLT15 trigger was fully efficient for $M_{jj} > 210$ GeV and the events selected by this trigger were used for the lowest M_{jj} region. The HLT30 was fully efficient for $M_{jj} > 320$ GeV and it was used for the $M_{jj} > 320$ GeV regions. We applied the phase space constraints $\chi_{\text{dijet}} < 16$ and $\mathrm{y_{boost}} < 1.11$. These requirements restrict the maximum rapidity of the two leading jets to $|\mathrm{y}_{max}| = 2.5$. After all selection cuts a sample of 6330 (3725) events remained for the $210 < M_{jj} < 320$ GeV ($M_{jj} > 320$ GeV) region.

The data are corrected for detector resolution effects, and the results are presented at the "particle level" (i.e., after hadronization). The correction factors were determined by a PYTHIA (D6T tune) MC sample passed through a full detector simulation and found to be less than 5% for all M_{jj} regions. As a conservative approach 100% of the correction factors were taken as systematic uncertainty.

The dijet angular distribution is relatively insensitive to many systematic effects; in particular it shows little dependence on variation of the overall energy scale. However, since χ_{dijet} depends on $\mathrm{y^*}$ directly, it is sensitive to the rapidity dependence of the jet energy corrections. The quadratic sum of the overall and η-dependent jet energy calibration uncertainties were found to be less than 5% to the χ_{dijet} distributions. The effect of the $\pm 10\%$ variation on the jet $\mathrm{p_T}$ resolution resulted in less than 2% uncertainty on the χ_{dijet} distributions.

The corrected dijet angular distributions, normalized to the total number of events within each M_{jj} region, are shown in Fig. 5. The different integrated luminosity used for the lowest M_{jj} region is because HLT15 trigger was prescaled during the running period at which the LHC was delivering higher instantaneous luminosity. The data are compared to pQCD predictions at next-to-leading order (NLO) calculated using fastNLO [14] based on NLOJET++ [15, 16]. Nonperturbative corrections due to hadronization and multiple parton interactions, determined

using PYTHIA (D6T tune) are applied to the prediction. The calculations were performed using the CTEQ6.6 PDFs [17]. The factorization and renormalization scales are set to the average dijet p_T. These scales were varied simultaneously from half to twice their central values and their effect to the NLO theoretical prediction, added in quadrature with the PDF uncertainties based on the 22 CTEQ6.6 uncertainty eigenvectors, are also shown in Fig. 5. Overall there is good agreement between the theoretical prediction and the data.

The sensitivity of the dijet angular distributions to a generic quark compositeness model represented by a four-fermion interaction additional to the QCD terms was investigated in Ref. [18]. The value of the mass scale, Λ, characterizes the strength of the quark substructure binding interactions and the physical size of the composite states. The contact interaction was introduced for left-handed quarks with constructive interference between the QCD and the new physics term with an effective Lagrangian: $L_{qq} = +\frac{g^2}{2\Lambda^2}(\bar{q}_L\gamma^\mu q_L)(\bar{q}_L\gamma_\mu q_L)$ [19].

The contributions from the contact interaction terms have only been calculated to LO, whereas the QCD predictions for the angular distributions are known up to NLO. The theoretical prediction used in the sensitivity study was constructed by multiplying the LO calculations for contact interactions bin-by-bin by the QCD $k-$factors ($k = \sigma^{NLO}/\sigma^{LO}$). Non-perturbative corrections due to hadronization and multiple parton interactions were also applied to the prediction. The effect of the contact interactions to the dijet angular distributions is depicted in Fig. 6 for a high M_{jj} region. Studies in Ref. [18] show that with a luminosity of ~ 2 pb^{-1} we expect to exclude the compositeness model with left-handed contact interference up to a scale of $\Lambda \sim 3$ TeV, starting to probe beyond the current Tevatron limit [3].

4 Summary

We have measured the differential dijet azimuthal distributions in several p_T^{max} regions and the dijet angular distributions in M_{jj} intervals. These are the first measurements of $\Delta\varphi_{\text{dijet}}$ and χ_{dijet} distributions in proton-proton collisions at 7 TeV. A data sample of 72 nb^{-1} from the early LHC running collected by the CMS experiment was used. The measured normalized $\Delta\varphi_{\text{dijet}}$ distributions are better described by the PYTHIA and HERWIG++ event generators. The MADGRAPH event generator predicts less azimuthal decorrelation than observed in the data. The measured χ_{dijet} distributions are well described by the NLO QCD calculations. The sensitivity of the dijet azimuthal distributions to the initial and final-state radiation was also illustrated. With an integrated luminosity of ~ 2 pb^{-1} we expect to probe a compositeness scale $\Lambda \sim 3$ TeV.

References

[1] M. G. Albrow et al., "Tevatron-for-LHC Report of the QCD Working Group", arXiv:hep-ph/0610012.

[2] DØ Collaboration, "Measurement of Dijet Azimuthal Decorrelations at Central Rapidities in $p\bar{p}$ Collisions at $\sqrt{s} = 1.96TeV$", *Phys. Rev. Lett.* **94** (2005) 221801.

[3] DØ Collaboration, "Measurement of Dijet Angular Distributions at $\sqrt{s} = 1.96TeV$ and Searches for Quark Compositeness and Extra Spatial Dimensions", *Phys. Rev. Lett.* **103** (2009) 191803.

[4] DØ Collaboration, "High-p_T Jets in $p\bar{p}$ Collisions at $\sqrt{s} = 630$ GeV and 1800 GeV", *Phys. Rev. D.* **64** (2001) 032003.

[5] CDF Collaboration, "Measurement of Dijet Angular Distributions at CDF", *[Erratum-ibid. **78**, 4307 (1997)] Phys. Rev. Lett.* **77** (1996) 5336.

[6] CMS Collaboration, "The CMS experiment at the CERN LHC", *JINST* **0803:S08004** (2008).

[7] M. Cacciari, G. P. Salam, and G. Soyez, "The anti-kt Jet Clustering Algorithm", *Nucl. Phys. B* **406** (1993) 187–224.

[8] CMS Collaboration, "Calorimeter Jet Quality Criteria for the First CMS Collision Data", *CMS PAS* **JME-09-008** (2009).

[9] T. Sjostrand, S. Mrenna, and P. Skands, "PYTHIA 6.4 Physics and Manual", *JHEP* **05** (2006) 026, arXiv:hep-ph/0603175.

[10] GEANT4 Collaboration, "G4–a simulation toolkit", *NIM* **A506** (2003).

[11] CMS Collaboration, "CMS Jet Performance in pp Collisions at $\sqrt{s} = 7$ TeV", *CMS PAS* **JME-10-003** (2010).

[12] M. Bahr et al., "Herwig++ Physics and Manual", *Eur. Phys. J.* **C58** (2008) 639–707, arXiv:0803.0883.

[13] J. Alwall et al., "MadGraph/MadEvent v4: The New Web Generation", *JHEP* **09** (2007) 028, arXiv:0706.2334.

[14] T. Kluge, K. Rabbertz, and M. Wobisch, "Fast pQCD calculations for PDF fits", in *14th International Workshop on Deep Inelastic Scattering (DIS 2006), 20-24 Apr 2006*, p. 483. Tsukuba, Japan, April, 2006. arXiv:hep-ph/0609285.

[15] Z. Nagy, "Three-jet cross sections in hadron hadron collisions at next-to-leading order", *Phys. Rev. Lett.* **88** (2002) 122003, arXiv:hep-ph/0110315.

[16] Z. Nagy, "Next-to-leading order calculation of three-jet observables in hadron hadron collisions", *Phys. Rev. D* **68** (2003) 094002, arXiv:hep-ph/0307268.

[17] P. M. Nadolsky et al., "Implications of CTEQ global analysis for collider observables", *Phys. Rev. D* **D78** (2008) 013004, arXiv:0802.0007.

[18] CMS Collaboration, "The CMS physics reach for searches at 7 TeV", *CMS Note* **2010-008** (2010).

[19] E. Eichten, K. Lane, and M. Peskin, "New tests for quark and lepton substructure", *Phys. Rev. Lett.* **50** (1983) 811.

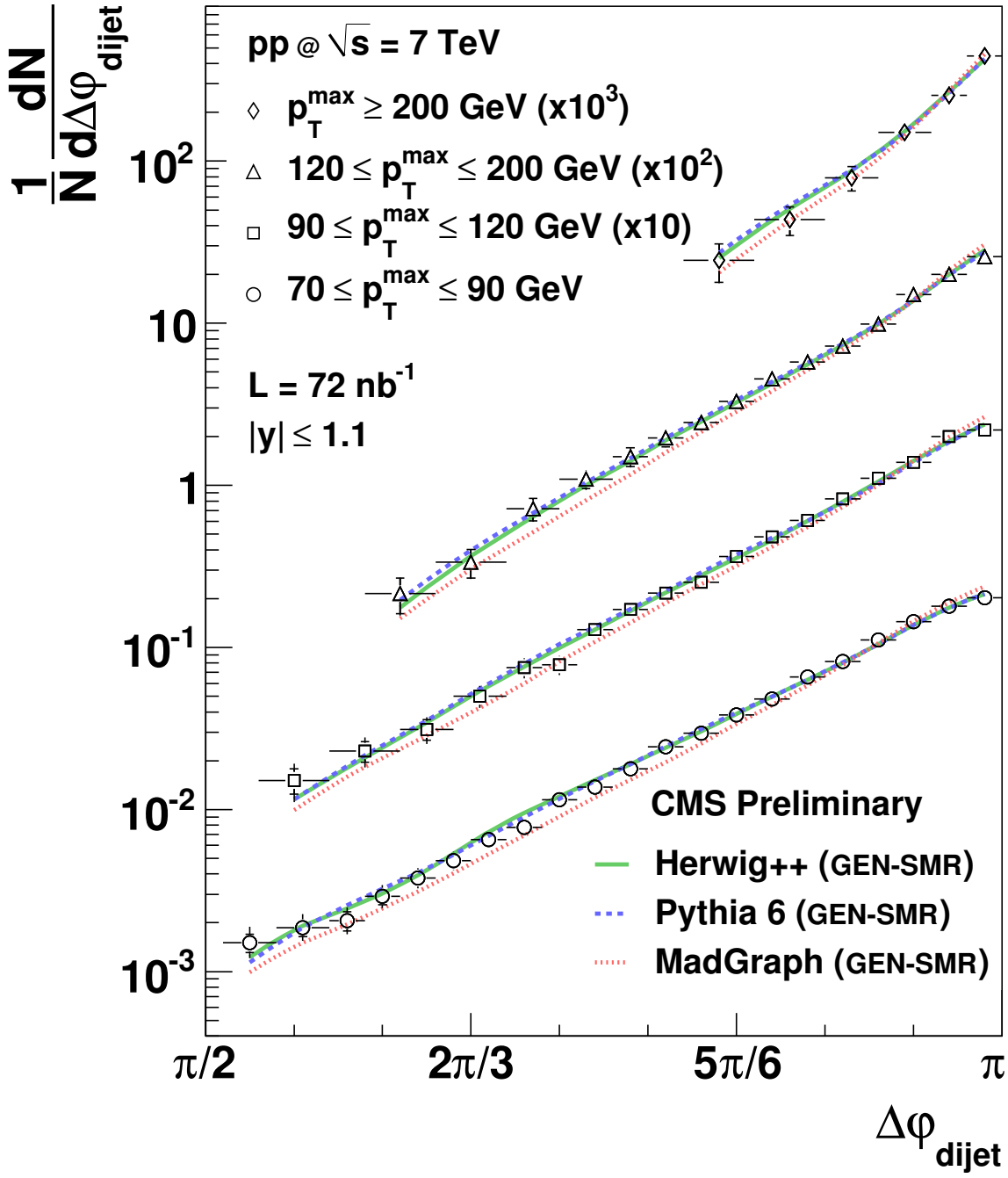

Figure 1: $\Delta\varphi_{\text{dijet}}$ distributions in different leading jet p_T^{max} regions. The curves represent predictions from PYTHIA, HERWIG++, and MADGRAPH. Detector resolution effects on jet p_T and position have been included in the MC predictions at the generated particle level (GEN-SMR). The data points include statistical (inner ticks) and systematic uncertainties.

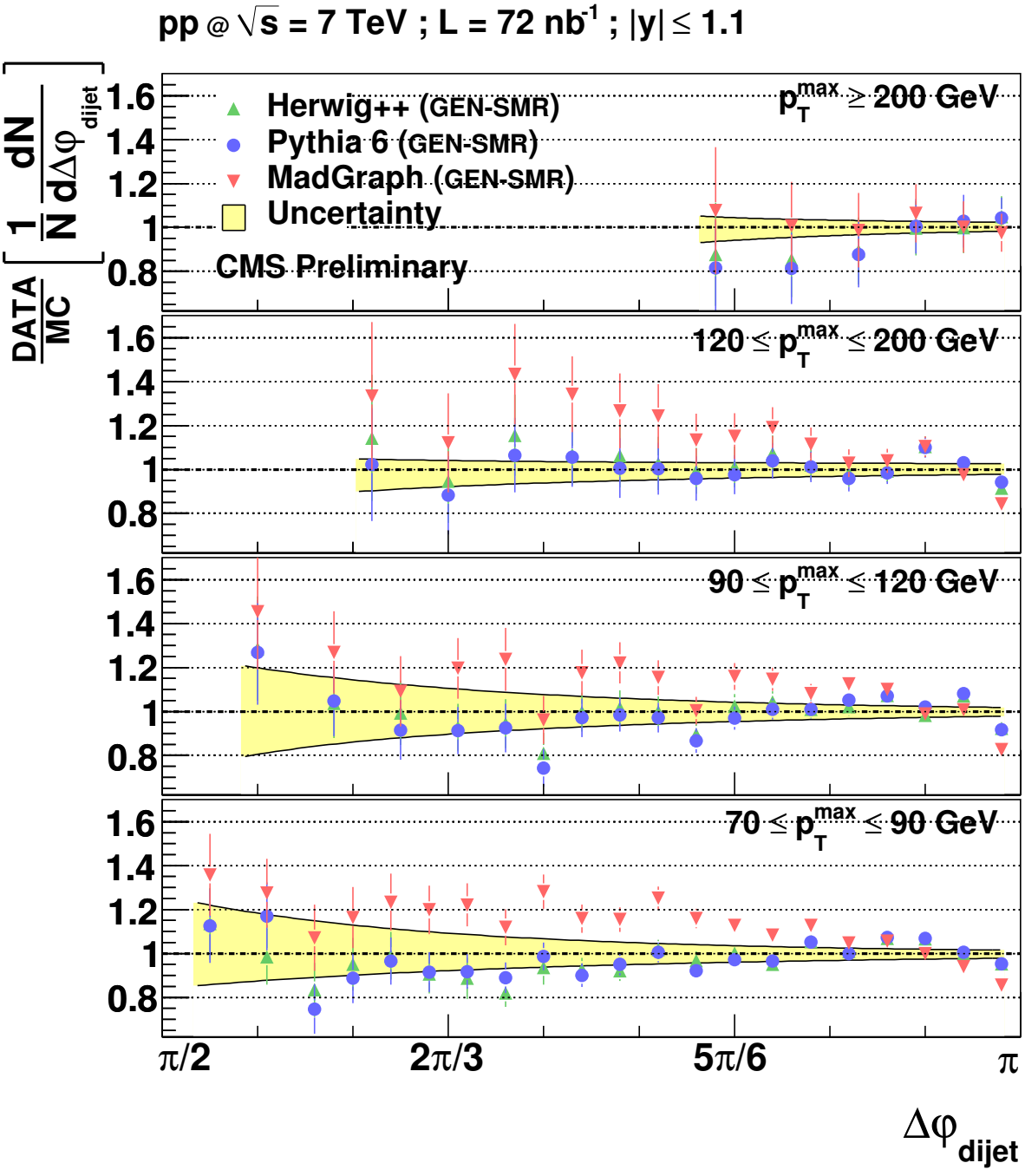

Figure 2: Ratios of data $\Delta\varphi_{\text{dijet}}$ distributions to PYTHIA, HERWIG++, and MADGRAPH predictions in different leading jet p_T regions. Detector resolution effects on jet p_T and position have been included in the MC predictions at the generated particle level (GEN-SMR). The shaded bands indicate the total systematic uncertainty.

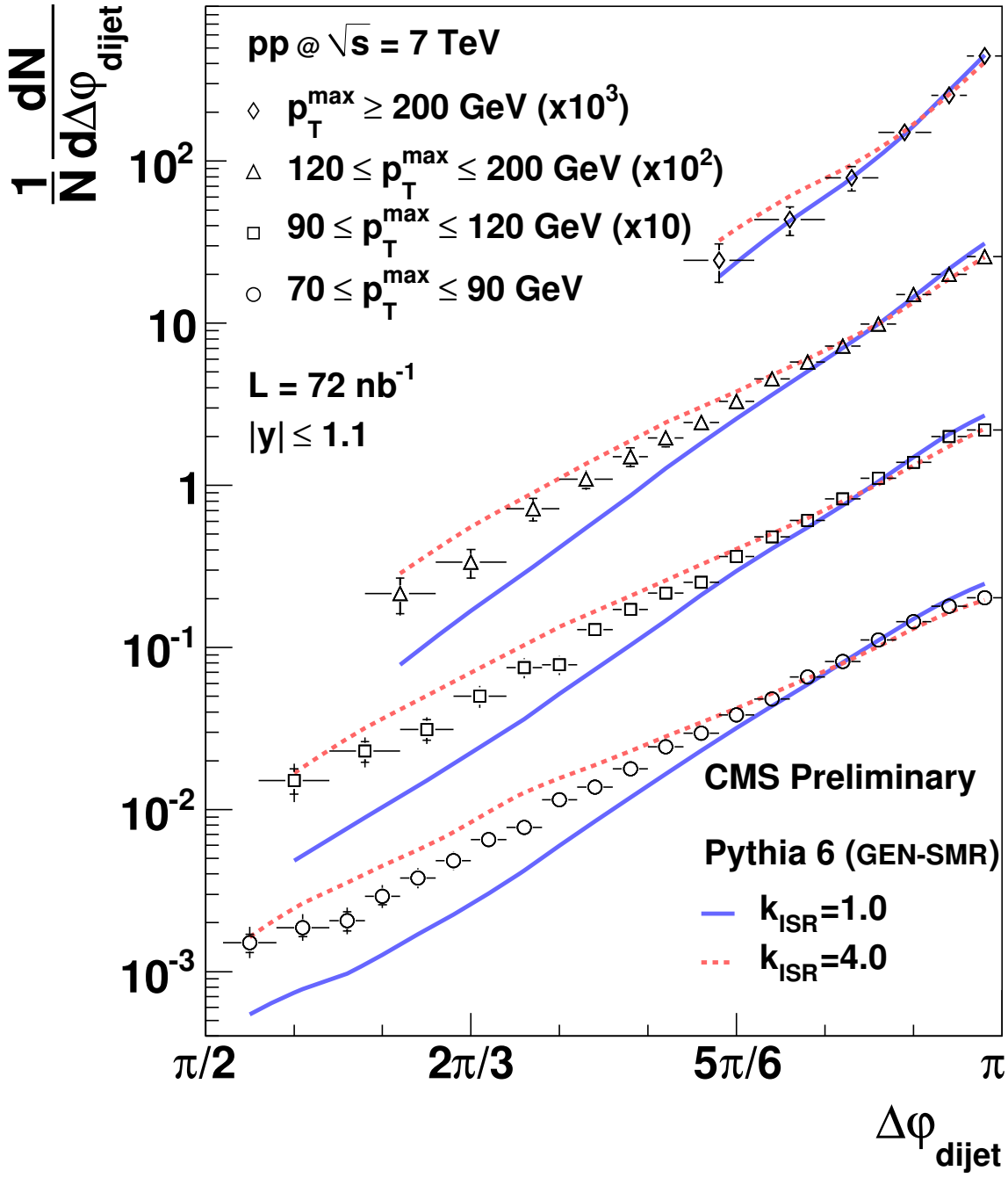

Figure 3: $\Delta\varphi_{\text{dijet}}$ distributions in different leading jet p_T^{max} regions. The curves represent the predictions from PYTHIA with $k_{ISR} = 1.0$ and PYTHIA with $k_{ISR} = 4.0$. Detector resolution effects on jet p_T and position have been included in the MC predictions at the generated particle level (GEN-SMR). The data points include statistical (inner ticks) and systematic uncertainties.

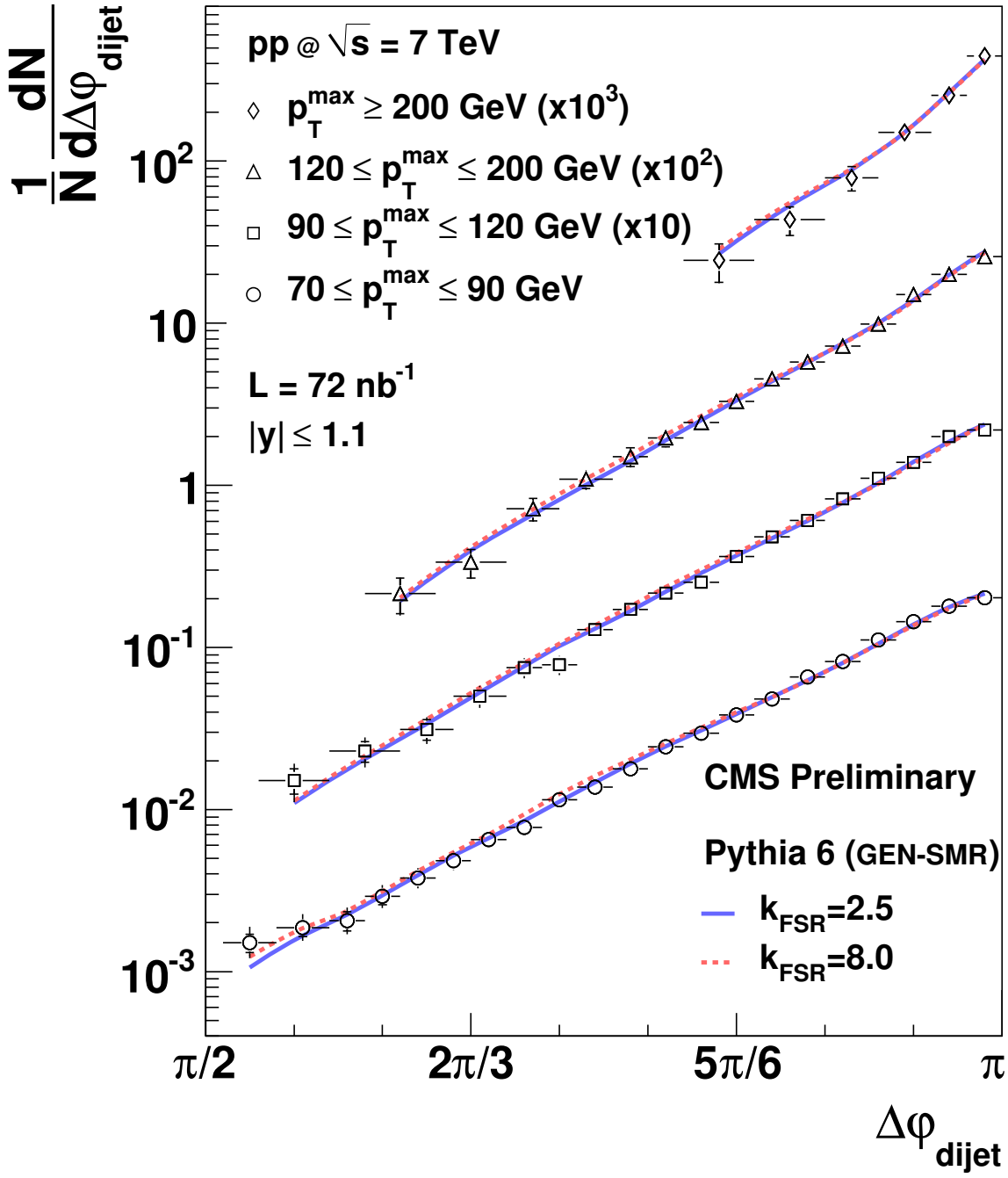

Figure 4: $\Delta\varphi_{\text{dijet}}$ distributions in different leading jet p_T^{max} regions. The curves represent the predictions from PYTHIA with $k_{FSR} = 2.5$ and PYTHIA with $k_{FSR} = 8.0$. Detector resolution effects on jet p_T and position have been included in the MC predictions at the generated particle level (GEN-SMR). The data points include statistical (inner ticks) and systematic uncertainties.

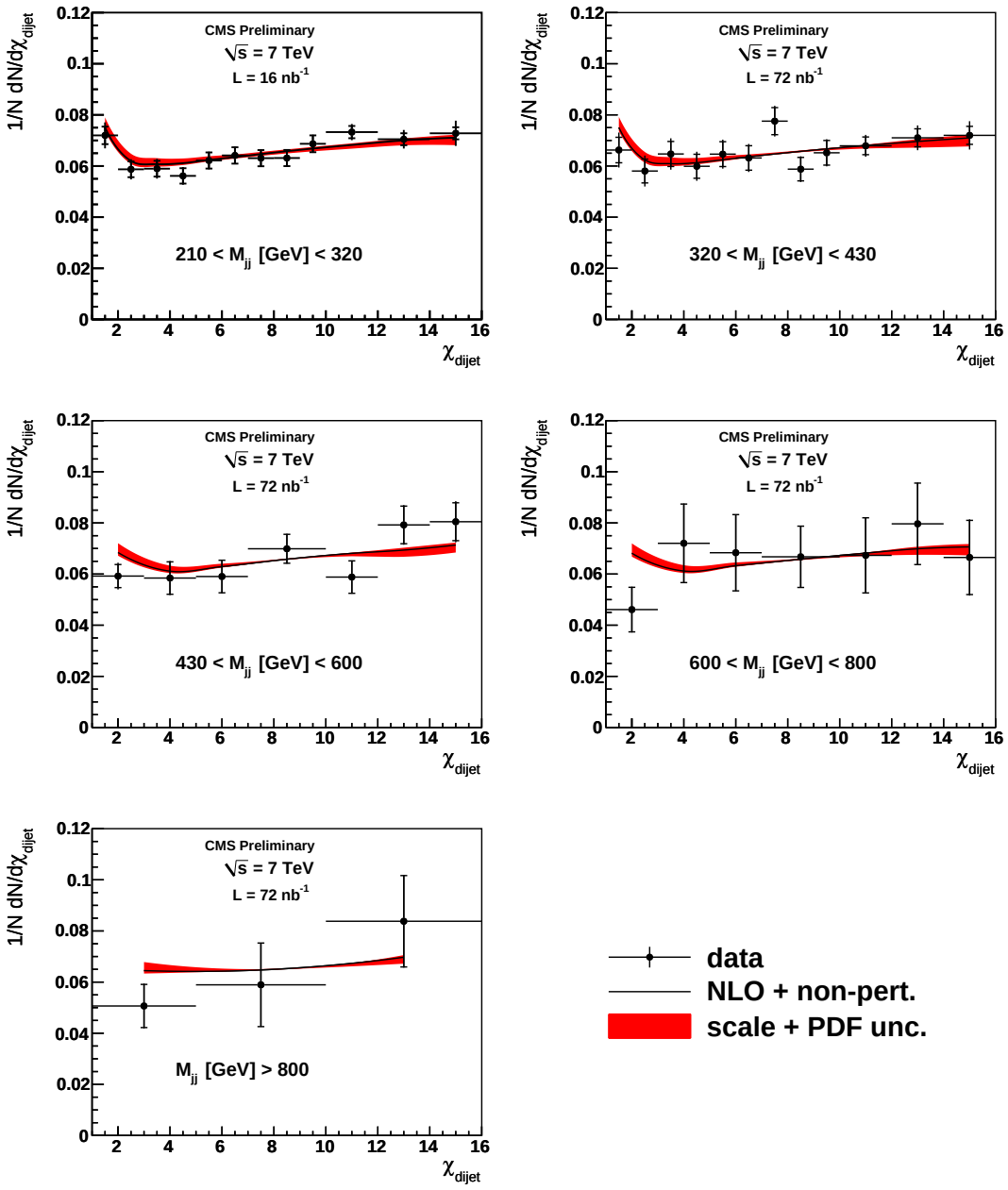

Figure 5: χ_{dijet} distributions in dijet invariant mass regions. The data distributions are compared to NLO QCD predictions including non-perturbative corrections. The data points include statistical (inner ticks) and systematic uncertainties. The theory band includes uncertainties from factorization and renormalization scale variations and the CTEQ6.6 PDF uncertainties.

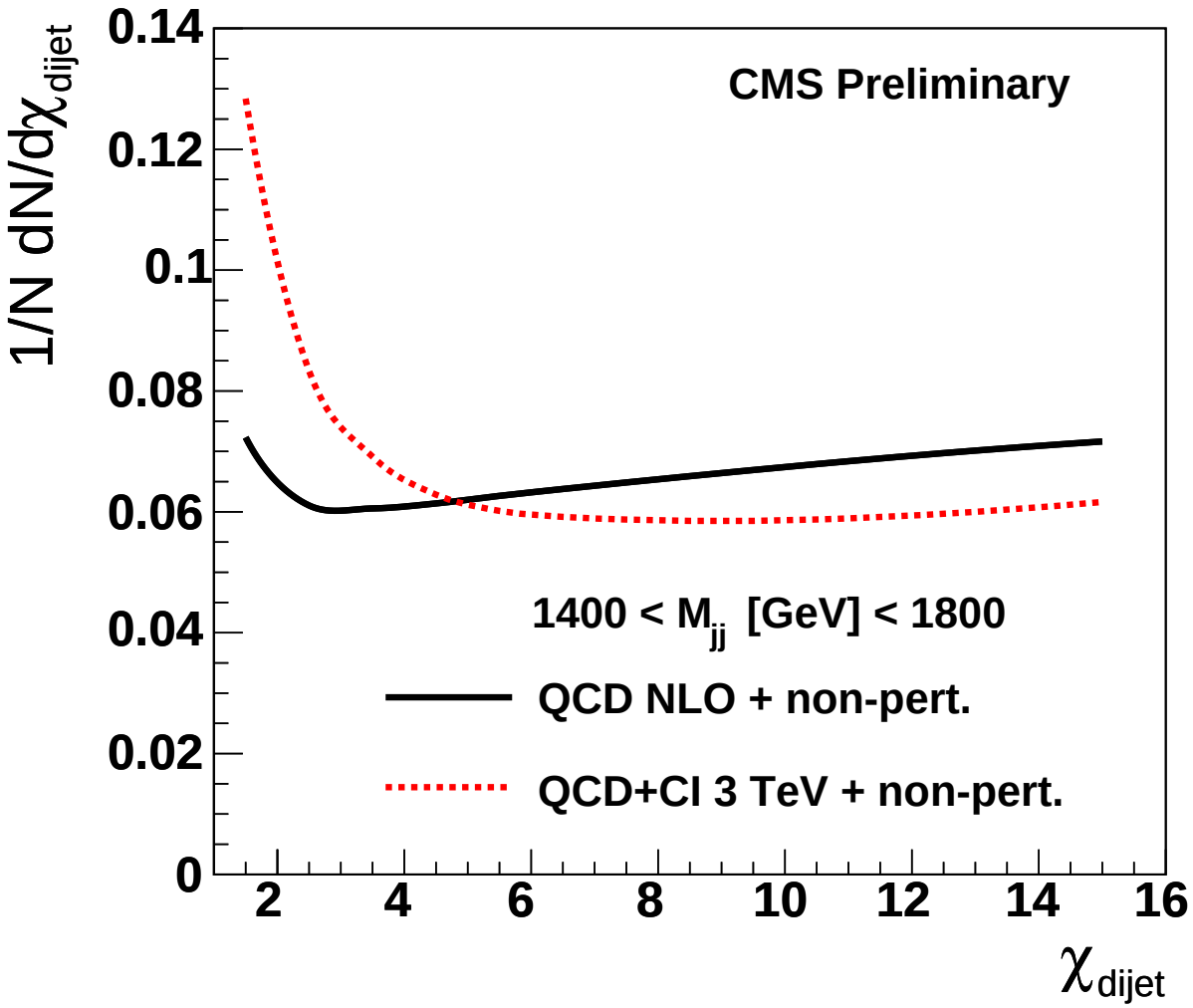

Figure 6: χ_{dijet} distributions for QCD and for QCD with contact interactions with mass scale $\Lambda = 3$ TeV. Non-perturbative corrections are applied to both theoretical predictions.